Institut "Jožef Stefan", Ljubljana

1000 Ljubljana, Jamova 39, pp 100 / Tel: 61 1259 199 / Fax: 61 1257 074 ali 61 219 385

IJS Report
IJS - DP - 7688
April 1997

HERA-B RICH Optical System Alignment with Data

A. Gorišek[a,b] and P. Križan[a,b]

[a] *"J. Stefan Institute, Ljubljana, Slovenia,*

[b] *Faculty of Mathematics and Physics, University of Ljubljana, Slovenia*

Abstract

In this report we present a method for alignment of the mirror segments in the RICH of HERA-B. The method uses recorded data, and was tested by using simulated events. The study shows that the mirrors can be aligned accurately enough to make the corresponding error in Čerenkov angle measurement negligible compared to the net error. The mirrors are aligned relative to a mirror segment which can be chosen arbitrary.

1 Introduction

Čerenkov photons that are emitted from a single track, are distributed on the detector area over a ring. If the mirror segments are not aligned perfectly, the centre of the photon ring will not coincide with the expected centre, the point which is determined by charged particle direction vector reflected on the ideal mirrors. (See Figs. 1 and 2). As a result, the Čerenkov angle, deduced from such a ring has an additional contribution to the error. It is the aim of this report to show, how this error can be reduced by using recorded data to a level far below the resolution.

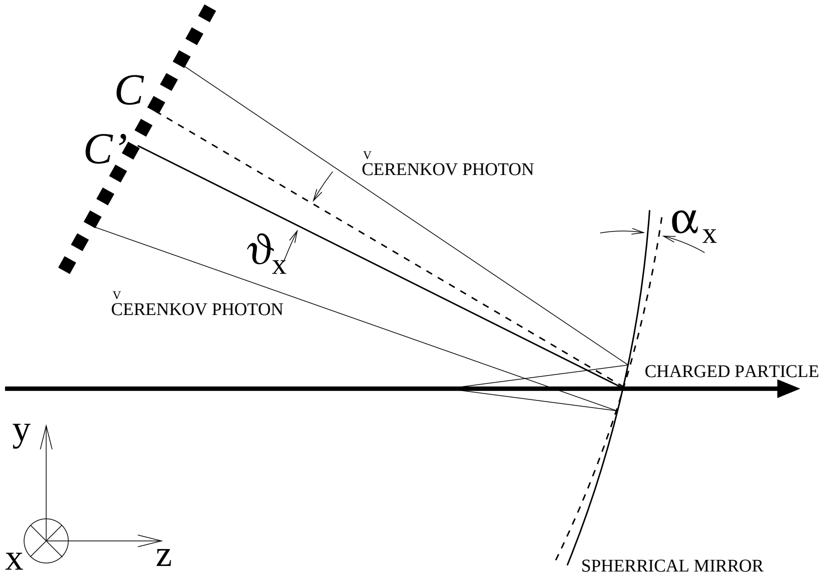

Figure 1: The dotted line represents the ideal position of the spherical mirror. If the mirror is displaced from the ideal position by an angle α, the centre of the Čerenkov ring C' will move by ϑ. The centre of the Čerenkov ring C' does not coincide with the point C which is determined assuming ideally positioned mirrors.

The measured Čerenkov angle (ϑ_{ch}) is the angle between the direction of photon hit on the photon detector and the direction of the centre of Čerenkov ring determined by ideally positioned mirrors (point C on Fig. 1). It can be plotted as a function of the polar angle about the charged particle direction (φ_{ch}). In case of ideally positioned optical system,

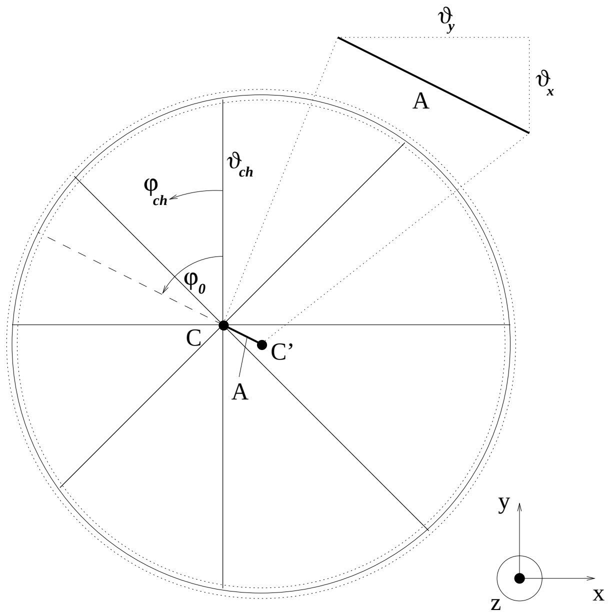

Figure 2: Čerenkov ring. The point C stands for the expected position of the ring centre, and C' is the actual centre.

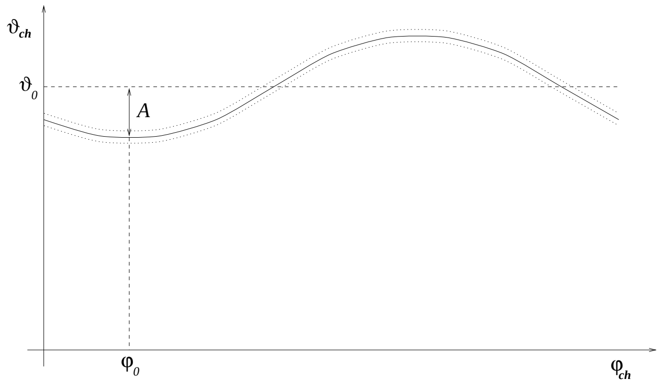

Figure 3: Measured Čerenkov angle ϑ_{ch} as a function of φ_{ch}.

the measured Čerenkov angle does not depend on the polar angle φ_{ch}, while otherwise, when the displacement from the ideal position is small compared with the mean Čerenkov angle, the measured Čerenkov angle ϑ_{ch} can be approximated by the following function of φ_{ch}:

$$\vartheta_{ch} = \vartheta_0 - A \cdot cos(\varphi_{ch} - \varphi_0) \tag{1}$$

This curve is represented in Fig. 3.

It is more convenient to write equation 1 in the following form:

$$\vartheta_{ch} = \vartheta_0 - A \cdot cos(\varphi_0) \cdot cos(\varphi_{ch}) + A \cdot sin(\varphi_0) \cdot sin(\varphi_{ch}) = \vartheta_0 - \vartheta_x \cdot cos(\varphi_{ch}) + \vartheta_y \cdot sin(\varphi_{ch}) \tag{2}$$

A misaligned optical system causes an additional error in the Čerenkov angle measurement that can be expressed in terms of standard deviation:

$$\begin{aligned} \sigma_\vartheta^{os} &= \sqrt{\langle(\vartheta_{ch} - \vartheta_0)^2\rangle} = \sqrt{\left(\frac{\partial\vartheta_{ch}}{\partial\vartheta_x}\right)^2 \cdot \sigma_{\vartheta_x}^2 + \left(\frac{\partial\vartheta_{ch}}{\partial\vartheta_y}\right)^2 \cdot \sigma_{\vartheta_y}^2} = \\ &= \sqrt{\cos^2\varphi_{ch} \cdot \sigma_{\vartheta_x}^2 + \sin^2\varphi_{ch} \cdot \sigma_{\vartheta_y}^2} \end{aligned} \tag{3}$$

In case of equal σ_{ϑ_x} and σ_{ϑ_y} the contribution to the error, σ_ϑ^{os}, will not depend on φ_{ch}:

$$\sigma_\vartheta^{os} = \sigma_{\vartheta_x} \tag{4}$$

The aim of optical system alignment is to reduce this contribution to the error. This is done in the following way. We first determine the parameters ϑ_x and ϑ_y by fitting the curve 2 to the measured data. Then the mirror segments are moved in such manner to reduce ϑ_x and ϑ_y to 0. This is achieved by turning the two adjustment crews on each mirror by the corresponding amount (Fig. 4). Note that there exists a linear relation between the rotation of the mirror mounting screws and the parameters ϑ_x and ϑ_y.

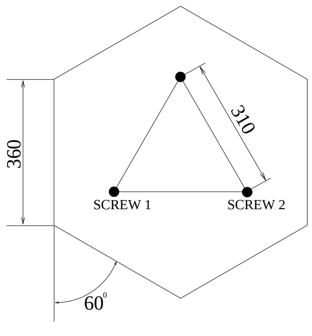

Figure 4: Each segment of the spherical mirror is of hexagonal shape. The segments of the spherical mirror and the planar mirror are both mounted in three points.

2 Unambiguous photons

Planar and spherical mirrors in the HERA-B RICH are both segmented. The enumeration of the segments as adopted in this report is shown in Figs. 5 and 6. Note that a somewhat simplified spherical mirror segmentation was used in this study (e.g. the real spherical mirror has a rectangular outer boundaries).

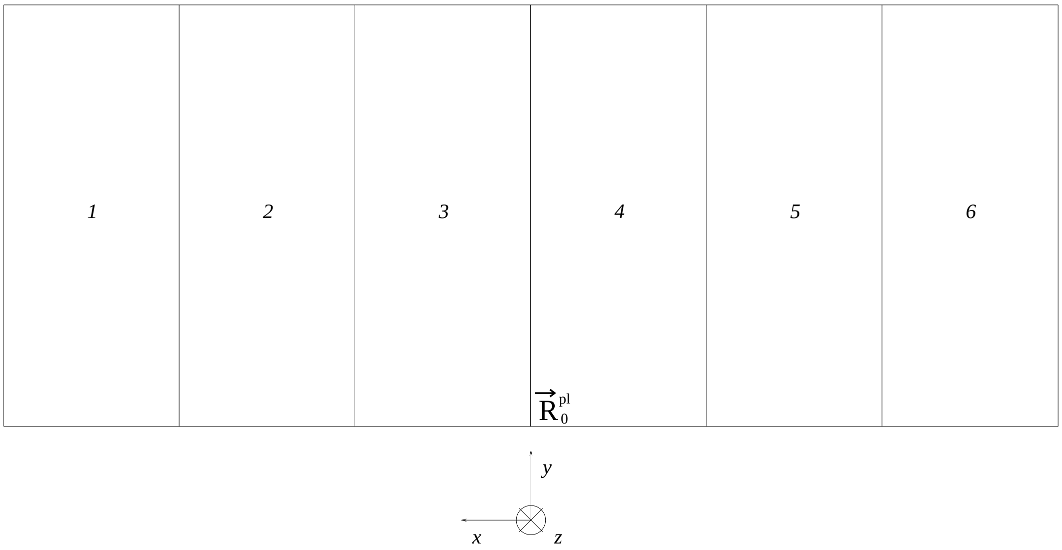

Figure 5: Planar mirror enumeration.

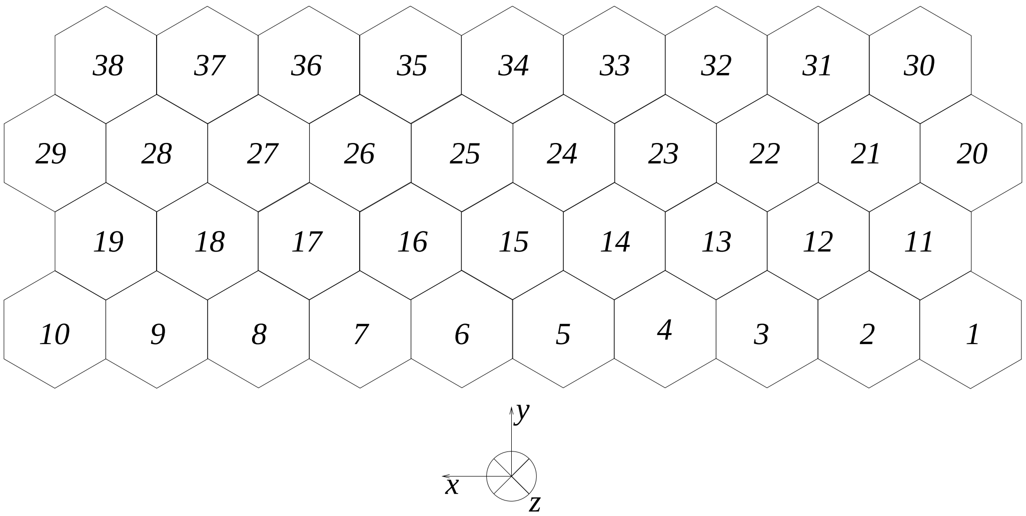

Figure 6: Spherical mirror enumeration.

In order to deduce the deviations of the orientations of the mirror segments one has to know on which mirror segment the photon was reflected. From the photon hit coordinate and the track direction it is possible to reconstruct the Čerenkov angle ϑ_{ch} and the polar angle about the track direction φ_{ch}. It is however impossible to deduce the point along the track path in the radiator in which the photon was emitted (Fig. 7). To check for possible ambiguities, we propagate through the optical system two auxiliary photons that are generated at the beginning of the radiator and at its end, both with the reconstructed values of the ϑ_{ch} and φ_{ch}. If both photons are reflected on the same spherical mirror segment, the same will hold also for the photons generated anywhere along the track direction in the radiator. The photon for which this is true is unambiguous Čerenkov photon. The same procedure is performed for the planar mirror. Only those photons, that are unambiguous on the spherical mirror and on the planar mirror, are considered in the process of deducing the mirror segment misalignment.

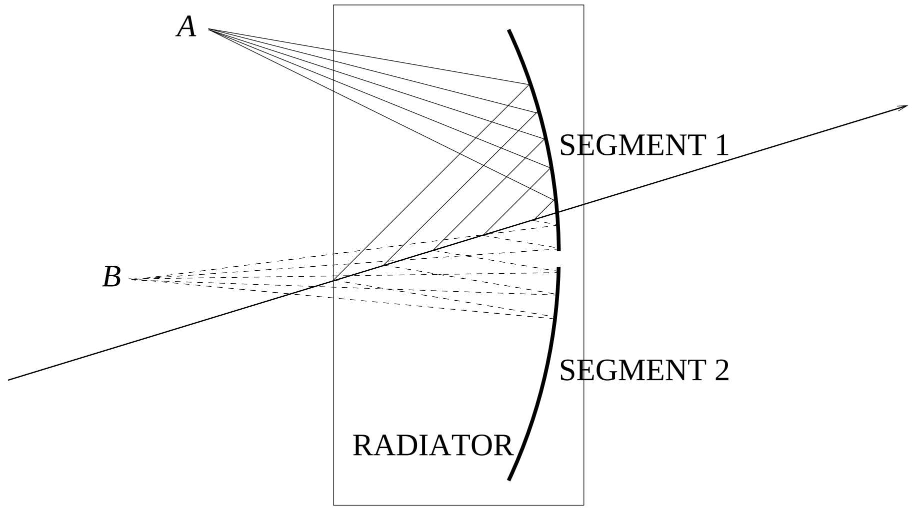

Figure 7: Unambiguous photons: The photon detected in the point A is unambiguous but that detected in the point B is not.

Note that in case of the optical system comprised of two mirrors that are both segmented it will often happen that the angle φ_{ch} will not cover the whole interval 2π (Fig. 8).

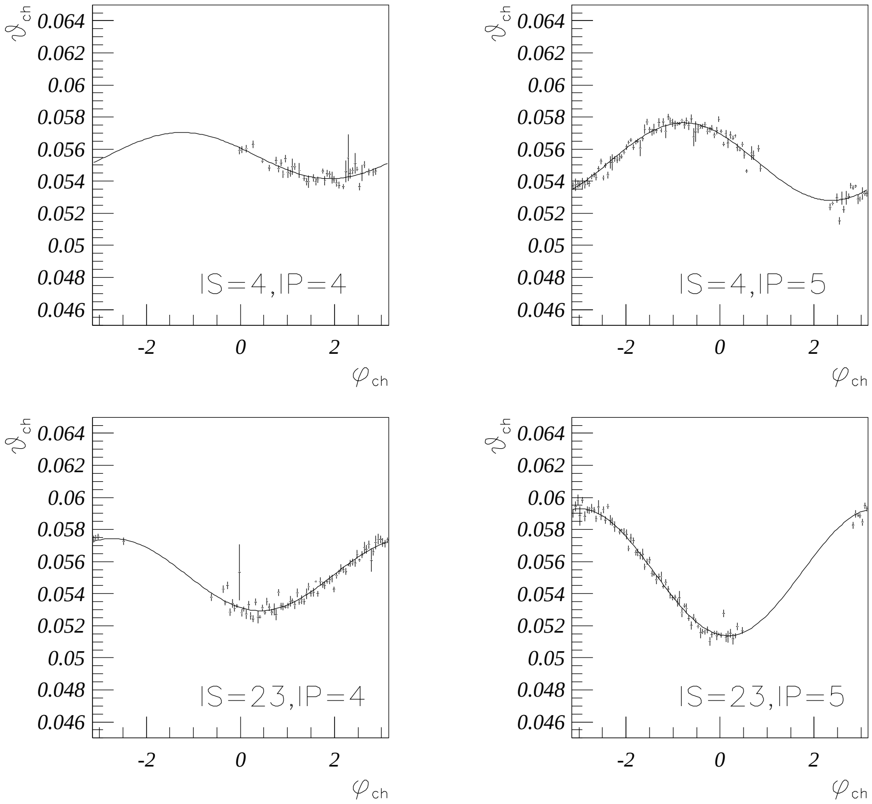

Figure 8: The full lines represent the fitted curves 2 to the data. The crosses mark the average of of the recorded data points in one part of the interval (the interval 2π of the angle φ_{ch} is divided into 128 parts). In neither case the angle φ_{ch} covers the full interval 2π. The numbers of mirror segments, to which the above pictures correspond to, are indicated beside each curve (IS is the number of the spherical mirror segment, Fig. 6, IP is the number of planar mirror segment, Fig. 5).

3 Linear system

In this section we present the method for the alignment of the optical system comprised of the spherical mirror divided into N parts and the planar mirror divided into M parts. The method is general and is not affected by the numbers of mirror segments.

By fitting the function 2 to the data we determine the displacement of the centre of Čerenkov ring on the photon detector, ϑ^x_{ij}, ϑ^y_{ij}, for each pair of the spherical mirror segment i and the planar mirror segment j that overlap, which means that there exist unambiguous photons that are reflected by the spherical mirror segment i and the planar mirror segment j. From the recorded Čerenkov ring on the photon detector only the sum of both displacements of the planar mirror and the spherical mirror can be deduced.

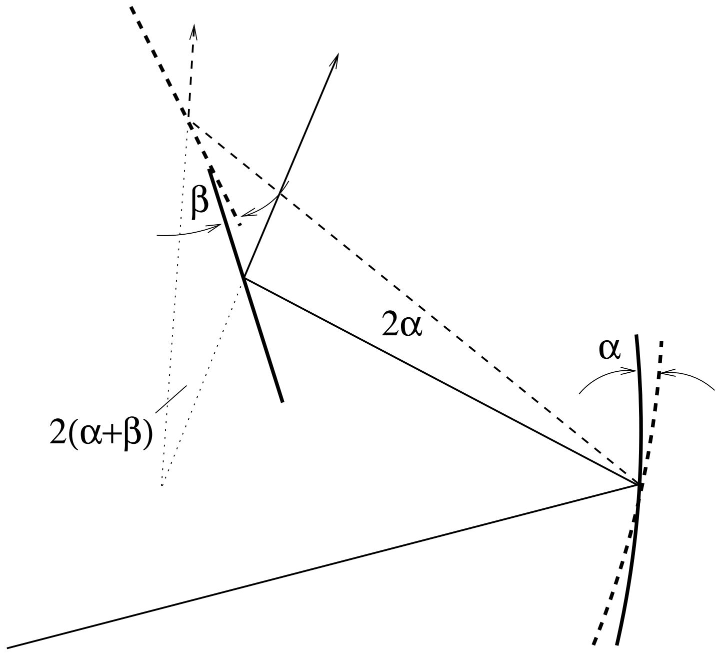

Figure 9: Reflection of a photon on the consecutive spherical and planar mirrors. The dashed line represents the path of the photon reflected on ideally positioned mirrors and the full line represents the unaligned system of mirrors.

The displacements of the Čerenkov ring on the photon detector: $\vartheta^x_{s\ i}$, $\vartheta^y_{s\ i}$, $\vartheta^x_{p\ i}$ and $\vartheta^y_{p\ i}$ are proportional to the displacements of the mirrors from the ideal positions (Fig. 9). The proportionality constants can be deduced from the length of the optical paths of photons from the spherical mirror to the photon detector and from the planar mirror to the photon detector (Fig. 10):

$$\vartheta^x_{s\ i} = a \cdot \alpha^x_i \tag{5}$$

$$\vartheta^y_{s\ i} = a \cdot \alpha^y_i \tag{6}$$

$$\vartheta^x_{p\ i} = b \cdot \beta^x_i \tag{7}$$

$$\vartheta^y_{p\ i} = b \cdot \beta^y_i \tag{8}$$

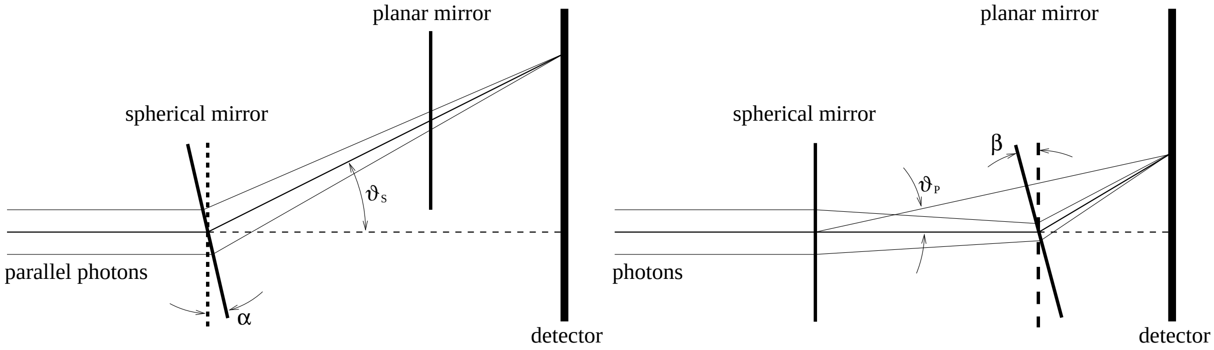

Figure 10: Picture shows schematically the effect of the displacement of spherical mirror segment, α, on the displacement of the Čerenkov ring, ϑ_s, and the effect of the planar mirror displacement, β, on the Čerenkov ring displacement, ϑ_p. The dashed line represents the case of the ideally positioned optical system.

The photon path from the spherical mirror to the photon detector is on average about twice as long as the photon path from the planar mirror to the photon detector. As a result, the effect of the planar mirror displacement is about twice smaller than the same displacement of the spherical mirror. The photon path lengths are not constant, so that the average proportionality constants $a = 1.98$ and $b = 1.05$ were determined by the simulation.

To determine the displacements of each mirror segment, we use the least square method. We should minimize the effect of the mirror misalignment on the picture on the photon detector. We should therefore minimize the following function:

$$\sum_{i,j} \frac{(\vartheta^x_{ij} - \vartheta^x_{s\ i} - \vartheta^x_{p\ i})^2}{\sigma^2_{x\ ij}} + \frac{(\vartheta^y_{ij} - \vartheta^y_{s\ i} - \vartheta^y_{p\ i})^2}{\sigma^2_{y\ ij}}, \tag{9}$$

ϑ^x_{ij} and ϑ^y_{ij} correspond to the parameters of the fitted curve 2, $\sigma_{x\ ij}$ and $\sigma_{y\ ij}$ are their standard deviations.

After the derivation of Eqn. 9 against the unknown parameters we get a set of linear equations:

$$\sum_i \frac{\vartheta^x_{ki} - \vartheta^x_{s\ k} - \vartheta^x_{p\ i}}{\sigma^2_{x\ ki}} = 0, \tag{10}$$

$$\sum_i \frac{\vartheta^y_{ki} - \vartheta^y_{s\ k} - \vartheta^y_{p\ i}}{\sigma^2_{y\ ki}} = 0, \tag{11}$$

$$\sum_i \frac{\vartheta^x_{ik} - \vartheta^x_{s\ i} - \vartheta^x_{p\ k}}{\sigma^2_{x\ ik}} = 0, \tag{12}$$

$$\sum_i \frac{\vartheta^y_{ik} - \vartheta^y_{s\ i} - \vartheta^y_{p\ k}}{\sigma^2_{y\ ik}} = 0, \tag{13}$$

This system can be more conveniently represented in a matrix form:

$$\underline{\mathbf{A}} \cdot \overrightarrow{\xi} = \overrightarrow{b}, \tag{14}$$

The vectors $\overrightarrow{b}$ and $\overrightarrow{\xi}$ have the following structure:

$$\overrightarrow{\xi} = \begin{Vmatrix} \vartheta^x_{s\ 1} \\ \vdots \\ \vartheta^x_{s\ N} \\ \vartheta^y_{s\ 1} \\ \vdots \\ \vartheta^y_{s\ N} \\ \vartheta^x_{p\ 1} \\ \vdots \\ \vartheta^x_{p\ M} \\ \vartheta^y_{p\ 1} \\ \vdots \\ \vartheta^y_{p\ M} \end{Vmatrix}. \tag{15}$$

$$\overrightarrow{b} = \begin{Vmatrix} P1_1 \\ \vdots \\ P1_N \\ P2_1 \\ \vdots \\ P2_N \\ R1_1 \\ \vdots \\ R1_M \\ R2_1 \\ \vdots \\ R2_M \end{Vmatrix}. \tag{16}$$

The elements of the vector $\overrightarrow{b}$ correspond to the x and y components of the displacements of the mirror segments. Their values are as follows:

$$P1_i = \sum_{j=1}^{M} \frac{\vartheta^x_{ij}}{\sigma^2_{x\ ij}} \tag{17}$$

$$
\begin{array}{c|cccc|}
 & N & N & M & M \\
\hline
N & S1 & 0 & \Sigma 1 & 0 \\
N & 0 & S2 & 0 & \Sigma 2 \\
M & \Sigma 1^T & 0 & T1 & 0 \\
M & 0 & \Sigma 2^T & 0 & T2 \\
\end{array}
$$

Figure 11: The form of the matrix of the linear system.

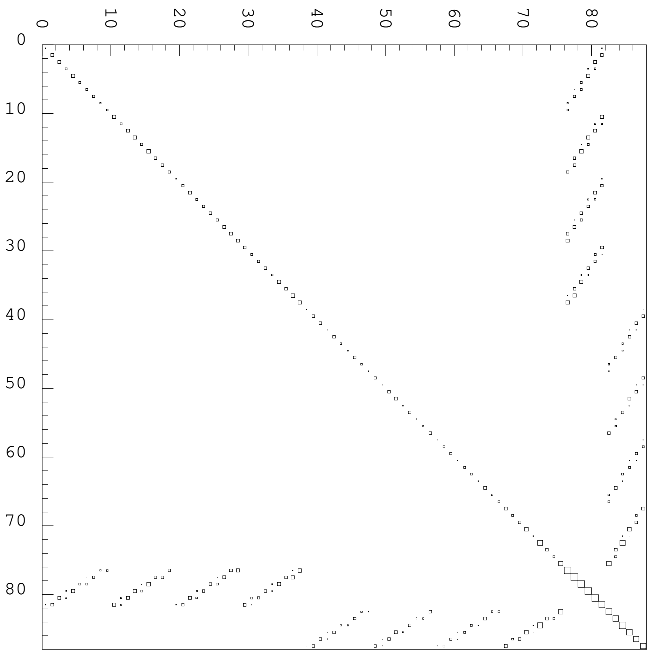

Figure 12: An actual matrix for the optical system comprised of 38 spherical and 6 planar mirror segments.

$$P2_i = \sum_{j=1}^{M} \frac{\vartheta^y_{ij}}{\sigma^2_{x\ ij}} \tag{18}$$

$$R1_i = \sum_{j=1}^{N} \frac{\vartheta^x_{ji}}{\sigma^2_{x\ ji}} \tag{19}$$

$$R2_i = \sum_{j=1}^{N} \frac{\vartheta^y_{ji}}{\sigma^2_{x\ ji}} \tag{20}$$

The matrix $\underline{\mathbf{A}}$ has the block form as presented in Fig. 11. Square matrices $S1$, $S2$, $T1$, $T2$ are diagonal. The diagonal elements have the following values:

$$S1_{ij} = \delta_{ij} \cdot \sum_{k=1}^{M} \frac{1}{\sigma^2_{x\ ik}} \tag{21}$$

$$S2_{ij} = \delta_{ij} \cdot \sum_{k=1}^{M} \frac{1}{\sigma^2_{y\ ik}} \tag{22}$$

$$T1_{ij} = \delta_{ij} \cdot \sum_{k=1}^{N} \frac{1}{\sigma^2_{x\ ki}} \tag{23}$$

$$T2_{ij} = \delta_{ij} \cdot \sum_{k=1}^{N} \frac{1}{\sigma^2_{y\ ki}} \tag{24}$$

Block matrices $\Sigma 1$ and $\Sigma 2$ have dimensions $N \times M$. Their elements differ from zero only in cases when the spherical mirror segment i overlaps with the planar mirror segment j. The matrices below the diagonal are just transposed matrices above the diagonal. They have the following values:

$$\Sigma 1_{i,j} = \sigma^{-2}_{x\ ij} \tag{25}$$

$$\Sigma 2_{i,j} = \sigma^{-2}_{y\ ij} \tag{26}$$

In Fig. 12 the matrix for our case is drawn on the histogram form. The area of squares is proportional to the value of the corresponding matrix element.

It makes no difference whether the mirror segments are aligned perfectly or if the planar mirror segments are all displaced in one direction and the spherical mirror segments in the other direction (Fig. 13) in such a way that their effects cancel. We have to choose one segment of the spherical or planar mirror and calculate the displacements of the other mirror segments relative to the chosen one. If we choose the spherical mirror segment k, the matrix $\underline{\mathbf{A}}$ will be reduced for all rows and columns belonging to this segment, namely the columns k and $N + k$ and rows k and $N + k$.

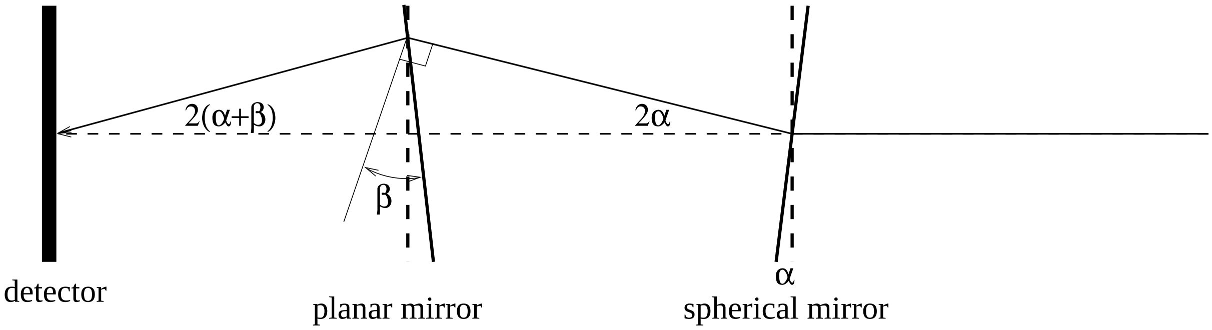

Figure 13: Symbolic figure representing the case when the effect of spherical mirror displacement is diminished by appropriate planar mirror displacement.

4 Isotropic distribution of charged particles

At first we tested the alignment method by using the simulated tracks that were distributed uniformly over the HERA-B solid angle. We generated 20000 tracks with 30 photons per track on average. That was enough for 30000 unambiguous photons that hit the upper photon detector.

We generated displacements of mirrors that were normally distributed with standard deviations of the displacements in both directions (x and y of mirror coordinate system) of 1 $mrad$ for spherical mirror segments and 2 $mrad$ for planar mirror segments.

In the Fig. 14 comparison between generated and calculated displacements is made.

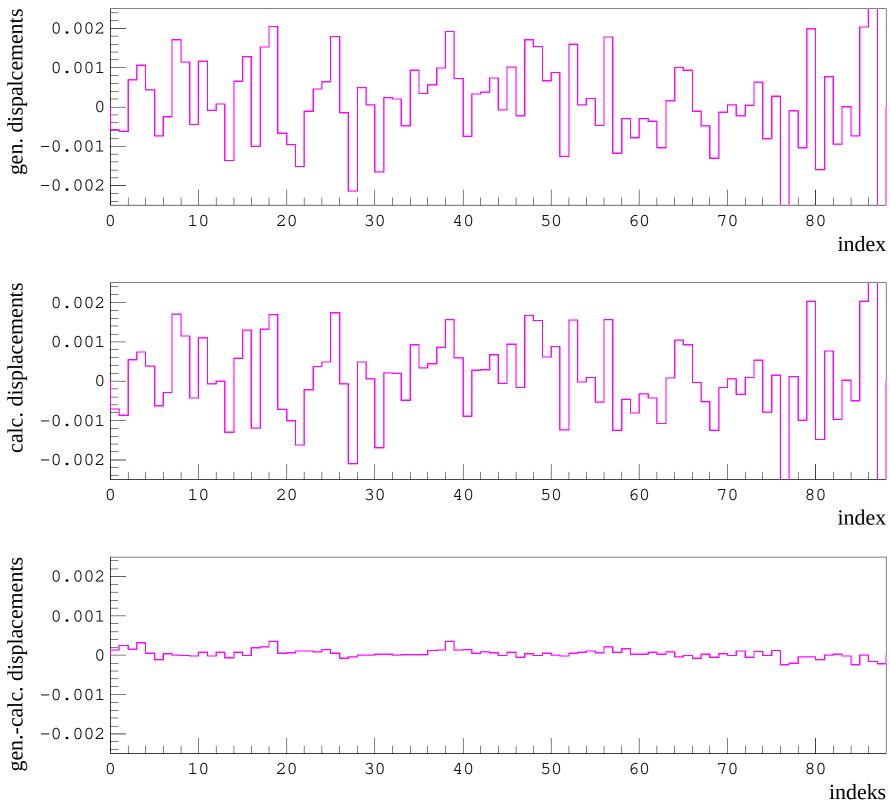

Figure 14: Generated displacements, calculated displacements and their differences. Index runs trough all coordinates of the spherical mirror and the planar mirror segments. Standard deviation of generated displacements is 1 $mrad$ for each coordinate.

4.1 Iterative method

The function 2 is only an approximation for the real problem. The coefficients a and b are not constant for all photons, since their path also differ slightly. As a consequence we will get better results if we repeat the alignment method with corrected mirror positions (Fig. 15).

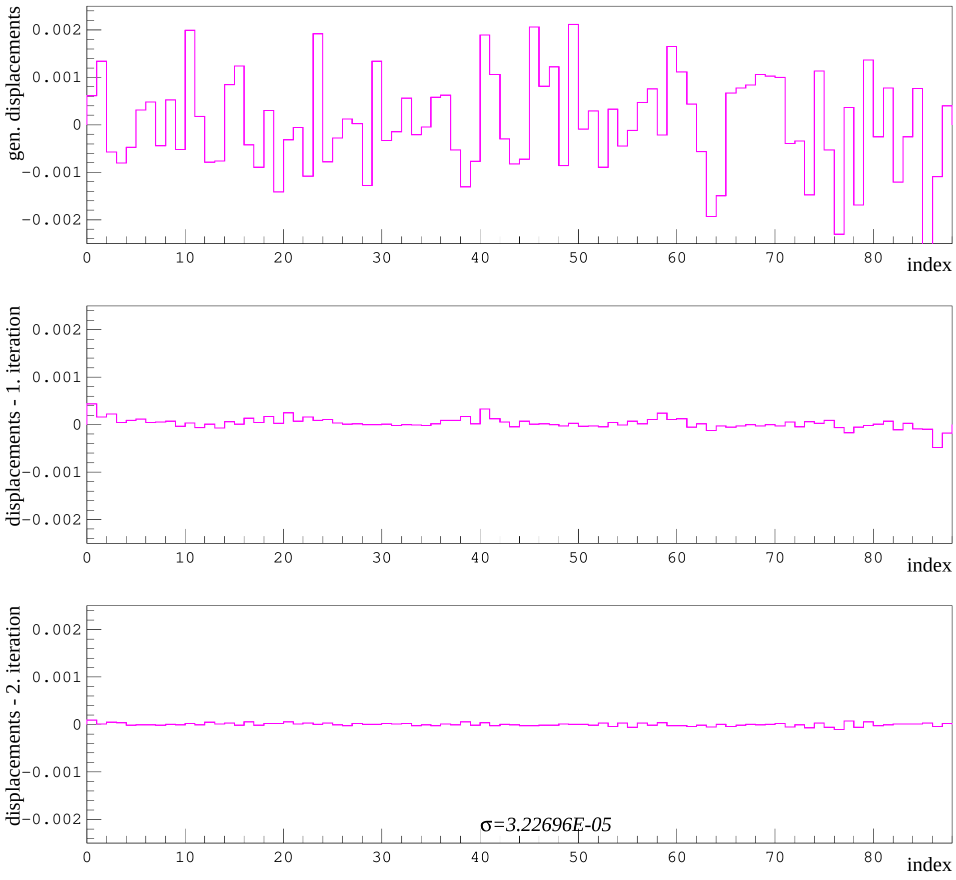

Figure 15: The comparison of the generated mirror displacements and the corrected mirror displacements after the first and after the second iteration of the alignment method. After the second iteration the standard deviation of mirror displacements is about 0.03 $mrad$.

After the second iteration of the alignment procedure we plot the amplitude ϑ_{ij} of the fitted function 2 for each pair of the planar mirror and spherical mirror segments that overlap. This give us a rough estimate for the error caused by the optical system misalignment. We present this amplitude in a two dimensional histogram (Fig. 17 and

18). Each spherical mirror segment can overlap with at most two different neighbouring planar mirror segments. In such cases two bins correspond to this spherical mirror segment in the plot. Otherwise there is only one bin for the given spherical mirror segment or in the worst case even none (when there is no unambiguous photons that were reflected on this mirror segment pair).

High bins belonging to spherical mirror segment i correspond to a very poor statistics of unambiguous photons because the two mirror segments in the pair overlap only slightly. In Fig. 16 we plotted the distribution of the amplitude ϑ_{ij} against the number of the unambiguous photons contributing to the given fit. It is important to note, however, that a large error in one combination is accompanied by a small one in the other combination connected to the same spherical mirror segment.

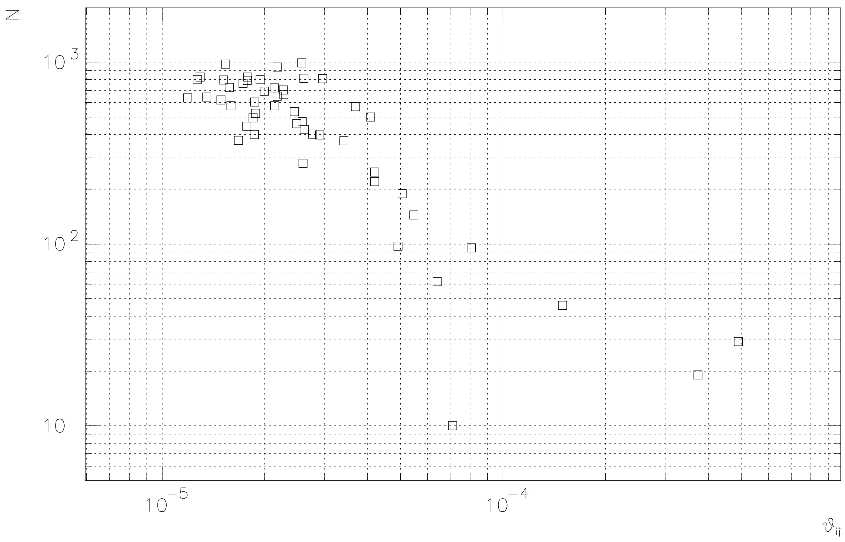

Figure 16: Distribution of the fitted amplitude ϑ_{ij} and the number of unambiguous photons that contribute to the fit. Each point corresponds to a bin in Fig. 17. Almost all unambiguous photons lie in the interval of ϑ_{ij} below 0.1 $mrad$. Both scales are logarithmic.

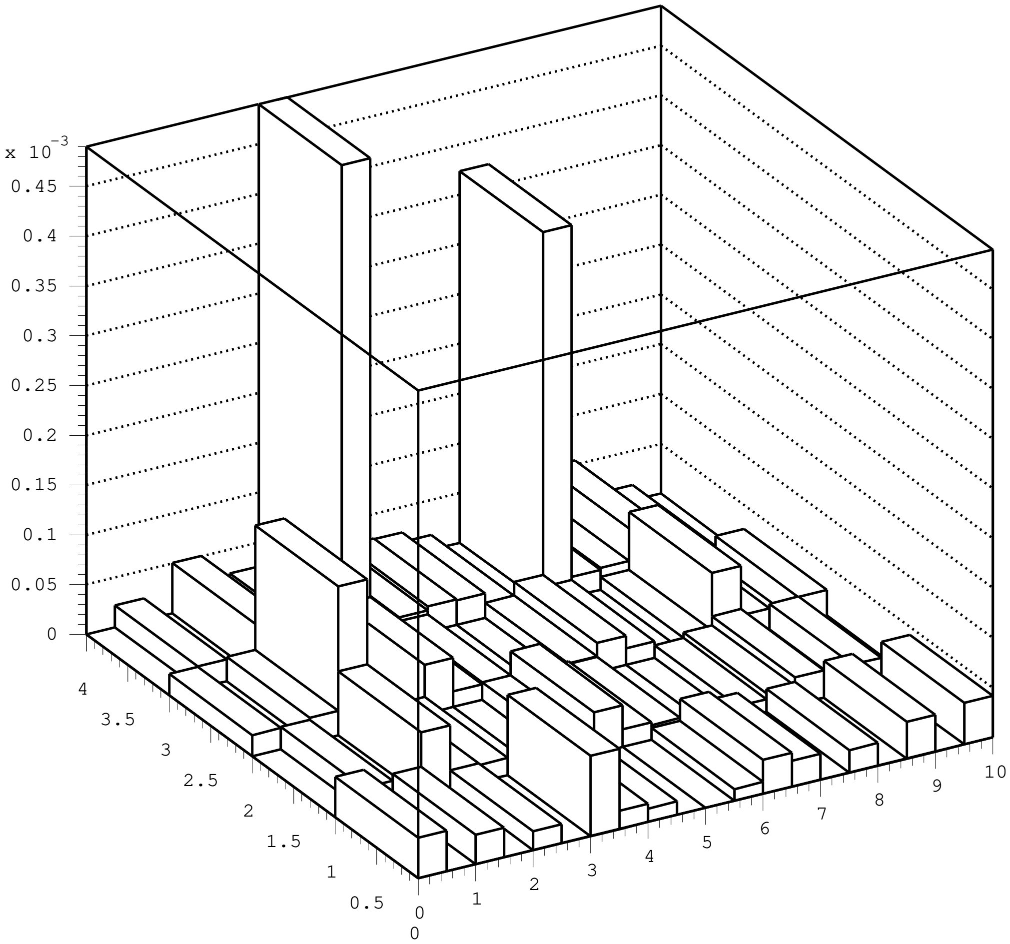

Figure 17: The fitted amplitude $\vartheta_{ij} = \sqrt{{\vartheta^x_{ij}}^2 + {\vartheta^y_{ij}}^2}$. The plot corresponds to the optical system after the second iteration of the alignment procedure. The heights of the bins correspond to the areas of the squares in Fig. 18. The numbers of the mirror segments to which the bins belong can be deduced from Fig. 18.

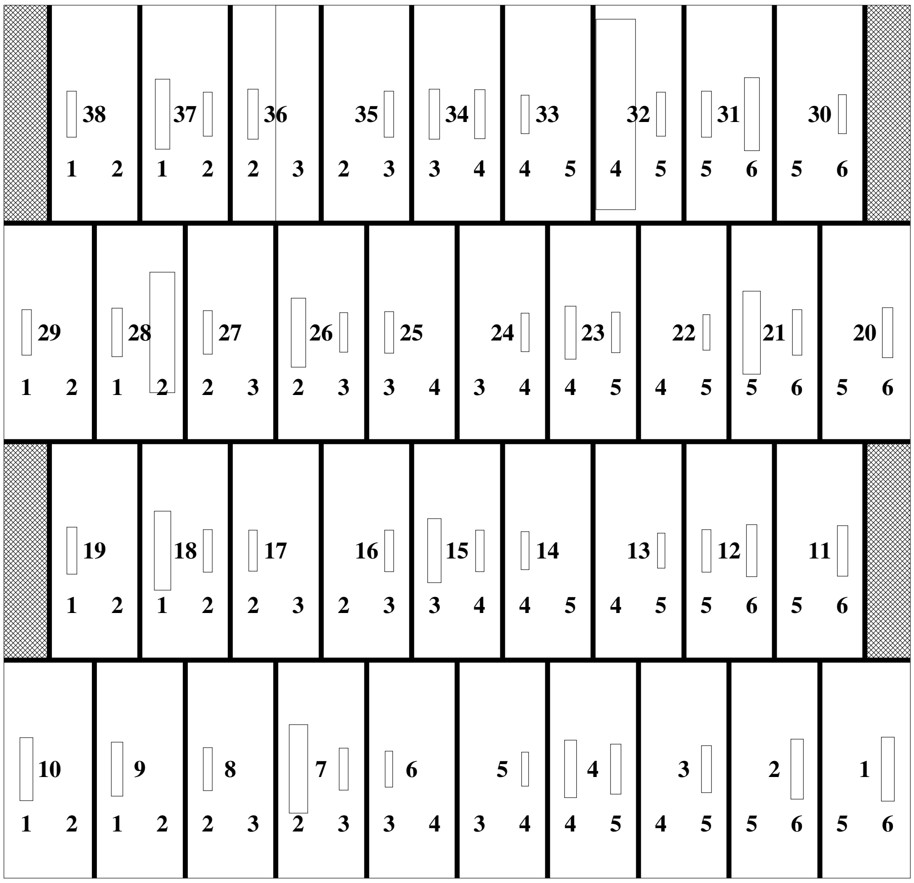

Figure 18: Same as Fig. 17.

4.2 Realistic charged particle distribution

The method was then tested by using the simulated events. An input to our alignment program was a file created by GEANT package, which contained the parameters of particles at the beginning of the radiator. The file contained a number of tracks that would be gathered during about 1 min of real HERA-B data acquisition. The charged pions and electrons with $p > 2.6\ GeV/c$ were chosen for the alignment. We used the first 50000 particles satisfying the above condition which gave about 50000 unambiguous photons on the upper photon detector.

At first we took the tracks to be isolated so that there was no overlap of the Čerenkov rings on the photon detector. This conditions can be approximately achieved by choosing only those events containing a small number of tracks. We deal with the general case containing the background in the next section.

Again we achieved better results by repeating the procedure of alignment with corrected optical system. The standard deviation of the mirror positions was below 0.05 $mrad$ after the second iteration of the alignment (Fig. 19).

Note that the particles from the GEANT file produced no unambiguous photons that would be reflected on the spherical mirror segments 1 and 20. These segments could not be aligned for the given (poor) charged particle statistics, as can be in Fig 19, variable $index$ 1,2 and 39,40.

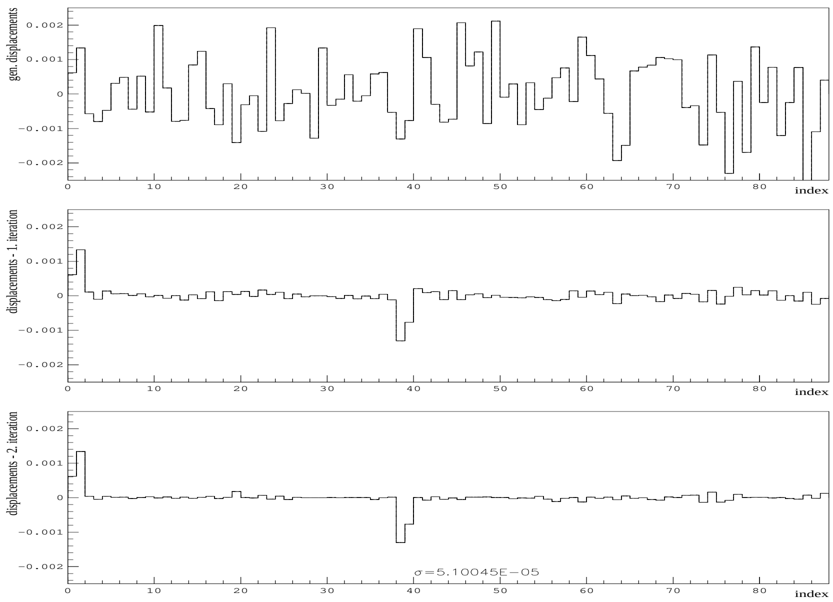

Figure 19: The comparison of the mirror segment positions. The upper figure represents the misaligned optical system, the figure in the middle represents the system after one alignment procedure and the third figure represents the system after the second iteration of the alignment.

4.3 Accounting for the overlap of the Čerenkov rings

In the previous section we used the isolated tracks for the optical system alignment. Those tracks caused Čerenkov rings on the photon detector that did not overlap with the rings of the other particles. In this case only the real Čerenkov photons contribute to the distribution of the measured Čerenkov angles ϑ_{ch} about the Čerenkov angles calculated from the velocity of the charged particles ϑ_0, as shown in the upper plot of Fig. 20.

In the average case about 350 particles enter the RICH radiator vessel during one proton bunch crossing through the target. Some of these particles radiate Čerenkov photons which then gather into rings on the detector. The overlapping of the rings is greater in the central region of the detector (the lower plot in Fig. 20) than it is at the detector's boundaries (the middle plot in Fig. 20).

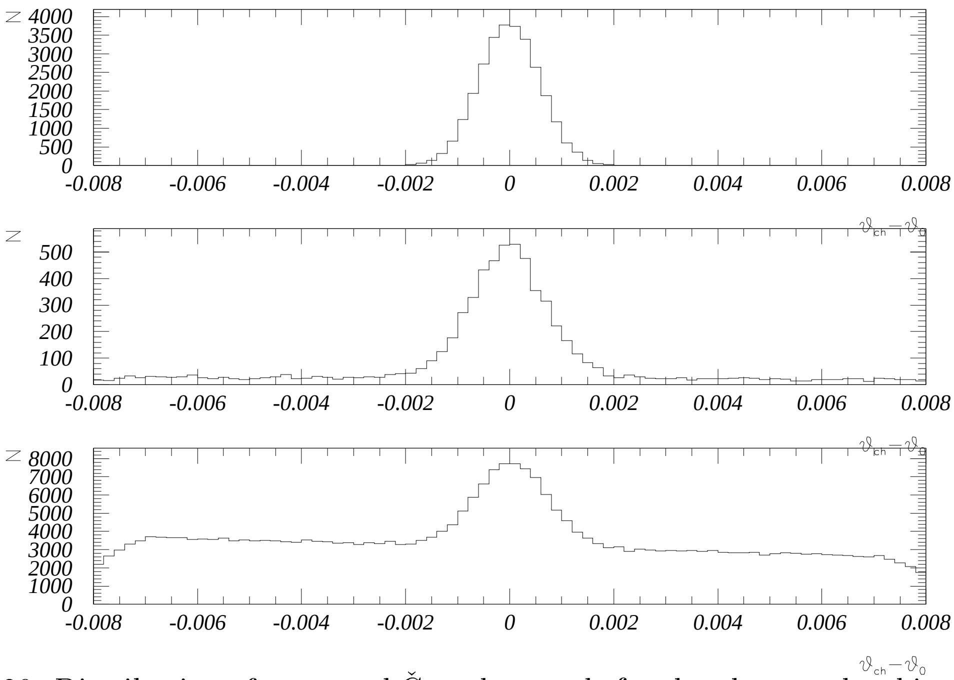

Figure 20: Distribution of measured Čerenkov angle for the photons that hit the detector. The upper plot represent the case of isolated tracks. The lower two plot correspond to the case where we account for the overlapping of the Čerenkov rings. The plot in the middle represent the photons that hit the boundaries of the detector and the lower plot represents the photons that hit the central region of the detector.

The background photons belonging to the neighbouring rings are distributed approximately linearly around the Čerenkov angle. To simulate the overlapping of the Čerenkov rings we generated besides the real Čerenkov also the corresponding number of background photons. The number of background photons depends on the region in which the photon hit the detector. The number of simulated background photons was proportional to the histogram in Fig. 22, which, in turn, was determined by the simulation [4].

We divided the two dimensional histogram of φ_{ch} and ϑ_{ch} into 30×30 parts for each

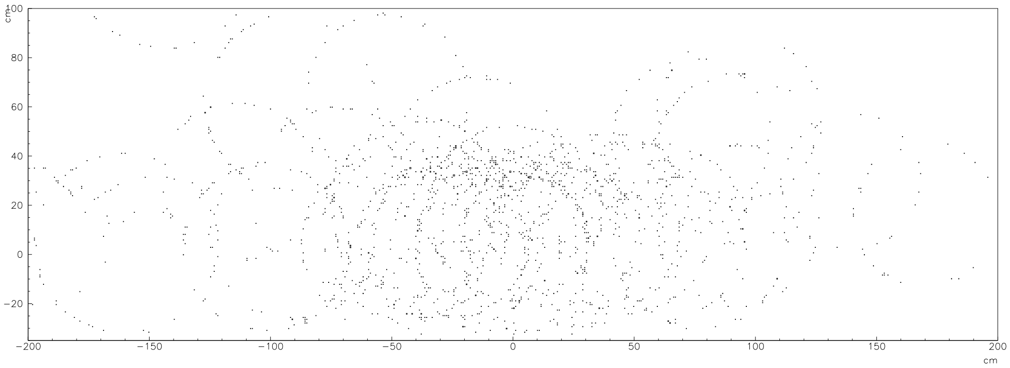

Figure 21: Typical RICH event on the upper detector.

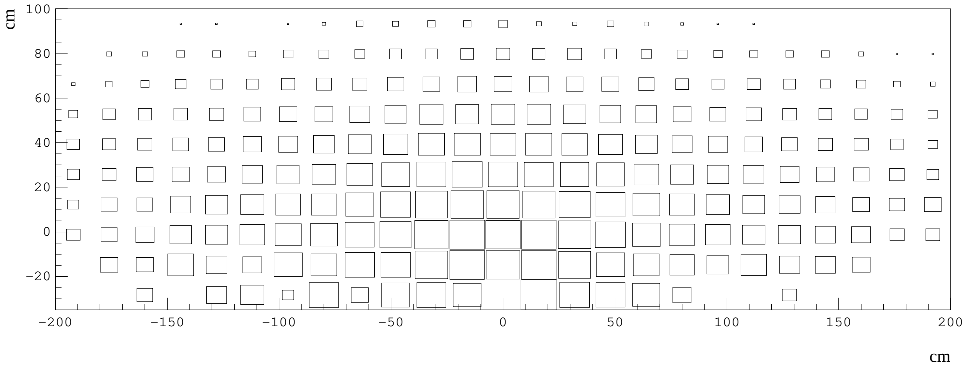

Figure 22: The distribution of the background over the upper photon detector. The level of background is much higher in the centre where the overlapping of the Čerenkov rings is greater.

pair of the planar and spherical mirror segments that overlap. We filled this histogram with the φ_{ch} and ϑ_{ch} of the reconstructed photons. Then the constant proportional to the maximum value of the histogram was subtracted from the histogram. All negative values were set to 0. The curve 2 is then fitted to the histograms obtained in this manner. In Fig. 23 we showed the subtracting of the background for the mirror segment pair composed of the planar mirror segment 4 and spherical mirror segment 4.

We repeated the alignment procedure three times since there was still a considerable improvement in the alignment of the optical system after the third iteration.

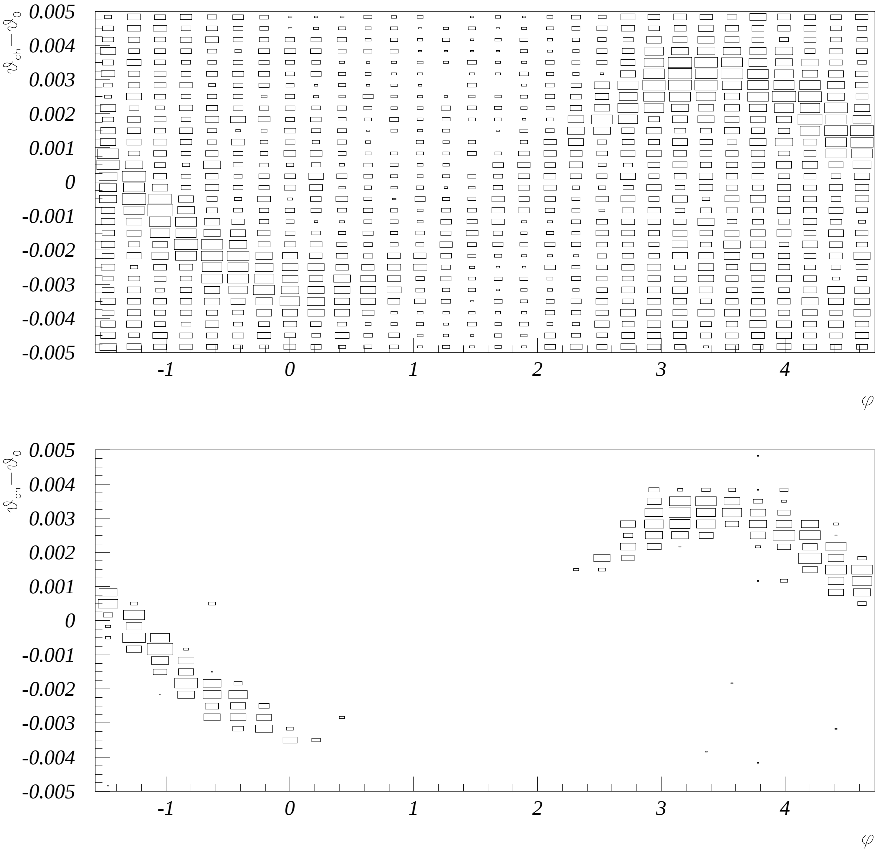

Figure 23: Plot shows the two dimensional histogram before and after the background was subtracted. The plot is drawn for the mirror segment pair composed of the planar mirror segment 4 and the spherical mirror segment 4.

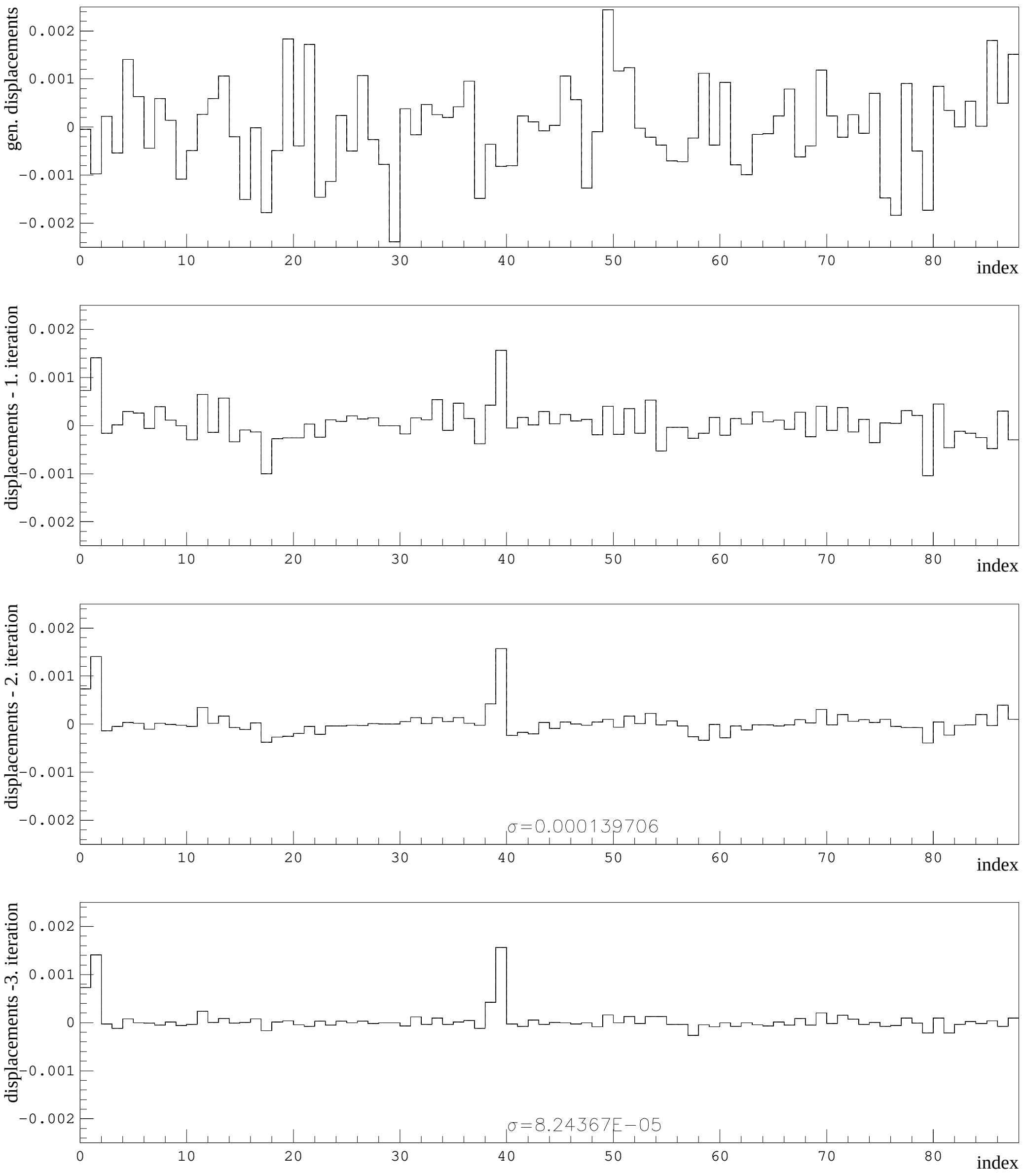

Figure 24: The comparison of the generated and the corrected displacements of the mirror segments after the first, the second and the third iteration of the alignment procedure.

4.4 The error in Čerenkov angle measurement

There are several independent contributions to the error in Čerenkov angle measurements. One of those contributions is the consequence of a misaligned optical system.

For the last case where we took into account the background due to the overlapping of the Čerenkov rings we draw the distribution of the difference between the measured Čerenkov angle and the Čerenkov angle determined by the particle velocity for all reconstructed photons. The distribution after the first, second and third iteration of the alignment gets closer and closer to the distribution of photons reflected on the ideally positioned optical system. The standard deviation of the distribution corresponding to the optical system after the third iteration of the alignment is $\sigma_D = 0.650\ mrad$ and that corresponding to the ideally positioned optical system $\sigma_E = 0.630\ mrad$. The contribution to the error in Čerenkov angle measurement after the third iteration is thus approximately $\sigma_\vartheta^{os} = \sqrt{\sigma_D^2 - \sigma_E^2} = 0.16\ mrad$.

The statistics of the charged particle that were considered was very poor. By increasing the statistics we expect that the contribution to the error due to optical system misalignment can be even further reduced.

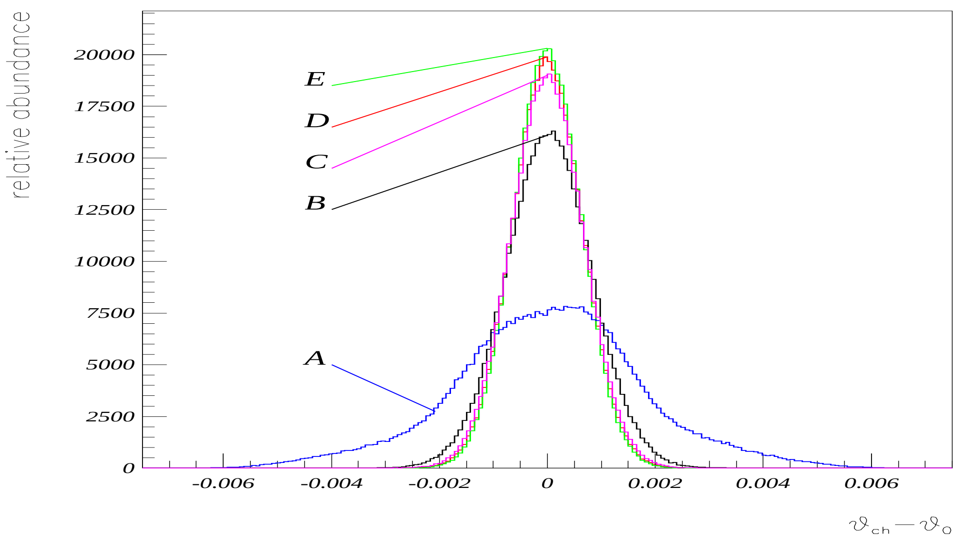

Figure 25: The distribution of the difference between the measured Čerenkov angle and the Čerenkov angle calculated from the velocity of the charged particle for all real Čerenkov photons that hit the photon detector. The broadest distribution A corresponds to unaligned optical system. The distributions B, C and D correspond to the aligned optical system after the first, second and third iteration of the alignment procedure. The distribution E corresponds to the photons that were reflected on the ideally positioned optical system.

5 Conclusion

We developed a method for alignment of the optical system comprised of two independent systems of mirrors like the one that will be installed in the HERA-B RICH radiator vessel.

First the method was tested by the simplest possible charged particle direction distribution, that is the isotropic distribution. Starting with 1 $mrad$ standard deviation in the starting distribution of the mirror segment directions we reduced it to approximately 0.03 $mrad$ after the second iteration of the adjustment procedure.

We tested the method also by using the GEANT produced particles with realistic distribution as expected in the real experiment. Starting with the same initial distribution of the mirror segment directions we reduced its standard deviation from initial 1 $mrad$ to 0.08 $mrad$ after the third iteration of the alignment procedure.

The alignment method is meant to be incorporated into ARTE package as a part of a slow control system, to monitor the mirror segment positions and to eventually align the optical system.

References

[1] A. Gorišek: Diploma thesis, University of Ljubljana, June 1997

[2] P. Križan, M. Starič, The optimal detector surface of a fixed target RICH with tilted mirror, Nucl. Instr. and Meth. A (1996) 124-129.

[3] Specification for Spherical HERA-B RICH Mirrors, 30 August, 1996

[4] P. Križan, T. Živko, IJS Report, IJS-DP-7456, Septrmber 1996.